
A&G
News and Reviews in Astronomy & Geophysics
June 2012 • Vol. 53 • Issue 3
Is the Sun going to sleep?
Mills Cross recalled • Robots vs astronauts
Earth observation matures

M. Lockwood, M.J. Owens, L. Barnard, C.J. Davis and S. Thomas
Solar cycle 24: What is the Sun up to?
Astron. & Geophys., 53 (3), 3.09–3.15, doi: 10.1111/j.1468-4004.2012.53309.x, 2012

Solar cycle 24: what is the Sun up to?

Mike Lockwood, Mat Owens, Luke Barnard, Chris Davis and Simon Thomas

(*Department of Meteorology, University of Reading, UK*)

March 2012 brought the first solar and geomagnetic disturbances of any note during solar cycle 24. But perhaps what was most remarkable about these events was how unremarkable they were compared to others during the space age, attracting attention only because solar activity had been so quiet. This follows an exceptionally low and long-lived solar cycle minimum, and so the current cycle looks likely to extend a long-term decline in solar activity that started around 1985 and that could even lead to conditions similar to the Maunder minimum within 40 years from now, with implications for solar-terrestrial science and the mitigation of space weather hazards and maybe even for climate in certain regions and seasons.

Predictions of the peak sunspot number during solar cycle 24 (SC24), made before it began, ranged from 42 to 185 [*Pesnell*, 2008] - a wide variation considering that observed values for SC13 to SC23 were between 65 and 208 (see Table). However, the minimum between SC23 and SC24 was, at least compared to other recent cycle minima, unusually deep and long-lived and solar activity has subsequently been very slow to recover. This can be interpreted in two ways: that SC24 will be similar to its predecessor but had an unusually delayed start, or that it started as usual but is weak. This discussion has important implications for solar and solar-terrestrial science and for the mitigation of space weather effects such as damage to and malfunction of satellite and aircraft electronics [*Dyer et al.*, 2003], health hazards in space [*Lockwood and Hapgood*, 2007] or during transpolar flights [*Mertens et al.*, 2010; *Barnard et al*., 2011], and disruption to power distribution networks [*Hapgood*, 2011]: in addition, all of the above have potential knock-on effects of lost service and lost industrial production and are of concern to the insurance and re-insurance industries [*Hapgood and Thompson*, 2010]. A weak cycle would be part of a long-term decline that began in 1985 [*Lockwood and Fröhlich*, 2007] that could return solar activity to levels last seen during the Dalton minimum (c. 1790-1830), or even the Maunder minimum (c.1655-1715) [*Lockwood et al.*, 2011]. *Lockwood* [2010] estimated that the probabilities of a return to Maunder minimum conditions within 40 and 150 years are 8% and 45%, respectively.

Long-Term Solar Change

Despite great advances in our understanding of the solar interior, made using the helioseismology technique, we do not yet have a predictive model of the solar dynamo [*Weiss and Thompson*, 2009]. As a result, we have to rely on analogue forecasts of solar activity based on past experience. Forecast skill is enhanced if longer data sequences are used as they increase the chance that the full range of potential behaviours has been included. The longest relevant data series come from cosmogenic radionuclides such as ^{14}C and ^{10}Be. These isotopes are produced by the bombardment of Earth's atmosphere by Galactic Cosmic Rays (GCRs) and are subsequently stored in terrestrial reservoirs, such as tree trunks and ice sheets. Earth is shielded from GCRs by the "open" solar magnetic field which is dragged out by the solar wind to surround the entire solar system and which rises and falls in response to solar activity [*Lockwood et al.*, 2009]. Hence, by measuring the cosmogenic isotope abundances in dateable cores taken from these reservoirs, the variation of solar activity over past millennia can be studied. The sunspot number R is an indirect measure of the magnetic flux generated by the solar dynamo which emerges through the solar surface. The open flux is the part of this emerged flux that also threads the top of the solar atmosphere and enters the heliosphere giving the interplanetary magnetic field (IMF). Sunspot number can be used to quantify the rate at which open flux is produced and the loss time constants are such that open solar flux and the IMF not only vary over the solar cycle, but also show long-term variability from one cycle to the next [*Lockwood et al., 1999; Solanki et al.*, 2000; *Owens and Lockwood*, 2012], with a considerable degree of predictability over several cycles [*Lockwood et al.*, 2011].

From ^{10}Be abundances, *Steinhilber et al.* [2008] generated a composite reconstruction of 40-year means of the heliospheric modulation potential ϕ_{40} over the past 9300 years; these have been interpolated to the 25-year values ϕ_{25} shown in figure 1 using cubic splines. This is a measure of the solar shielding of GCRs and is highly correlated with 25-year means of open solar flux, sunspot number and other solar activity indicators, including the aa geomagnetic activity index. Recent decades form one of 24 peaks in these ϕ_{25} data which are termed "Grand Solar Maxima" (GSMs). *Abreu et al.* [2008] noted that the recent GSM has lasted longer than any other in this record and deduced that its end was overdue, a conclusion supported by *Lockwood et al.* [2009] from the trends in open solar flux and historic geomagnetic activity data. The yellow dashed lines in figure 1 mark the ends of GSMs, defined to be when ϕ_{25} exceeds 610 MV.

The Long-Term Space Weather Forecast

It is often stated that solar activity is inherently unpredictable, but *Lockwood et al.* [2011] have used autocorrelation functions to show that the persistence of open solar flux and the heliospheric modulation parameter is high enough to give some predictability over 3 or 4 solar cycles, sufficient to foresee the onset of a grand minimum in activity.

Figure 2 shows a composite of the ϕ_{25} values around the times of the GSM endings defined in figure 1. It can be seen that there is great variability in the behaviour and that after 2 of the 24 GSMs, ϕ_{25} fell to the Maunder Minimum level (the horizontal dashed line in figure 2) within 40 years. Extrapolation over the 12.5 years since the last available data point gives ϕ_{25} at the recent minimum of the solar cycle to be 610 MV. Adopting this to be the threshold for defining a grand maximum means that the recent GSM has just ended, provided that values of ϕ in SC24 remain lower than the corresponding SC22 values at the same solar cycle phase (given that the 25-year running means ϕ_{25} cover two solar cycles). Data from neutron monitors show that this is definitely the case thus far during SC24, with GCR counts giving consistently and considerably lower ϕ and so we can be increasingly confident that the recent GSM (defined using this threshold ϕ_{25}) has come to an end. *Lockwood* [2010] used figure 2 to evaluate the probability of ϕ_{25} evolving to various levels by a given time. *Barnard et al.* [2011] added decadal-scale solar cycles to these predictions by evaluating the variation of the fractional deviation of annual means ϕ_1 from ϕ_{25} (i.e., $(\phi_1-\phi_{25})/\phi_{25}$) as a function of solar cycle phase, ε. The value of ε was predicted into the future by assuming all solar cycles will have the average duration of 11.1 years. Hence for a predicted ϕ_{25} and ε, the annual mean, ϕ_1, could also be predicted. In addition, *Barnard et al.* extended the predictions to sunspot number using a linear regression between ϕ_{25} and R_{25} and then applying the corresponding analysis of $(R_1-R_{25})/R_{25}$ with ε. They also predicted annual IMF values the same way.

The coloured lines in the top panel of figure 3 shows the resulting predictions for annual mean sunspot number R, extending the observed record (in black) into the future. The other panels show the results of applying the same procedure to the near-Earth IMF field strength, B, the Oulu neutron monitor cosmic ray counts and the aa geomagnetic index, respectively. The aa index is compiled for 1868 onwards and direct observations of B from satellites are available only after 1963. Annual means of B have been derived from historic geomagnetic data [*Lockwood et al.*, 2009, *Lockwood and Owens*, 2011] and these are shown by the mauve line in the second panel and the mauve line in the third panel is the reconstruction of cosmic ray counts by *Usoskin et al.*

[2002] that is also ultimately based on the geomagnetic data. The predictions employ the threshold ϕ_{25} of 610 MV (as discussed above) to define a GSM and assume that all future cycles last 11.1 years. The coloured lines are for constant probabilities of *R*, *B* and aa being lower than the y-axis values, *P*[<*R*], *P*[<*B*] and *P*[<aa], respectively. There is only a 5% probability of cycles maintaining an amplitude as large as SC23 (*P*[<*R*] = 95%, top, red line) and there is a 5% probability of reaching Maunder minimum levels within 40 years (*P*[<*R*] = 5%, bottom, blue line). The most likely evolution is roughly midway between these two extremes. The predicted cycles in *B* and aa are similar to those in *R*, but are superposed on a long-term decline which mirrors that in the open solar flux, as does the rise in cosmic ray fluxes.

Comparison of The Present and Past Solar Cycles

Which of the predicted future variations shown in figure 3 is consistent with the evolution of SC24 thus far? To answer that question we have to define how far into the cycle we now are. Since the start of the regular observations of sunspot latitude in 1844 at Greenwich, the average value ($<\lambda_{spots}>$, the centre of the "wings" in the famous "butterfly diagram" [*Hathaway*, 2010]) has evolved with solar cycle phase ε in very similar manner in all cycles [*Owens et al.*, 2011]. To compute ε, the start/end time of each cycle is here taken to be when $<\lambda_{spots}>$ increases rapidly as the new-cycle, high-latitude spots first dominate over the old-cycle, low-latitude spots. This is close to the time of minimum sunspot number but much easier to define accurately. The points in figure 4(a) show monthly $<\lambda_{spots}>$ as a function of ε, colour-coded by cycle number. The black line shows that SC24 is following the same variation if it is assumed to end early in 2019. From this, we estimate that we have now (1st May, 2012) reached a cycle phase of $\varepsilon = 120°$. The Table shows that, on average, solar maximum has been at phase $\varepsilon_{max} = 125 \pm 19°$. This yields a prediction that the peak of SC24 will be during calendar year 2012 and so could even have been reached already.

The estimate of the cycle phase of $\varepsilon = 120°$ is supported by observations of the Heliospheric Current Sheet (HCS) tilt shown in figure 4(d). We here use the HCS tilt index devised by *Owens et al.* [2011], as derived from potential field source surface (PFSS) mapping of magnetograph data from the Wilcox Solar Observatory (WSO) magnetograph. The index is defined as the fraction of source surface grid cells which have opposite field polarity (radial) field to their immediate longitudinal neighbours, thus quantifying the degree to which the HCS is warped. This index is only available for 1976 and after and so only covered cycles SC21-SC23 before the present one. Figure 4(d) shows that the current phase of $\varepsilon = 120°$, as deduced from $<\lambda_{spots}>$, is also consistent with the HCS tilt data, at least for SC21 onwards, as the recent HCS tilt is as high as was seen around the sunspot maxima of SC21, SC22 and SC23.

The other indicator that can be used to define where we are in the current cycle is the polarity of the solar polar magnetic field. The timing of the polar field reversal, relative to sunspot maximum, was first observed during SC19 by *Babcock* [1959] using data from the Hale Solar Laboratory (HSL) magnetograph. He noted that the average field emerging from the south solar pole reversed polarity between March and July 1957 and that in the north pole reversed in November 1958. The12-month running mean of monthly sunspot number peaked in March 1958, midway between these two reversals. Figure 5 employs the continuous data on the solar polar field available from WSO. As noted by Babcock during SC19, the two poles do not reverse at exactly the same date, and the raw data are also complicated by a strong annual periodicity introduced by the annual variation in Earth's heliographic latitude. Because of these two effects, the average polar field reversals are most readily seen by taking the difference between the north and south fields, (B_N–B_S). In order to give the variations of this difference the same appearance in each cycle, thereby allowing easy comparisons, the upper panel of figure 5 shows (B_N–B_S) multiplied by p, where p = +1 for odd-numbered cycles and p = –1 for even ones: the variation of $p(B_N–B_S)$ with solar cycle phase, ε (determined the same way as in figure 4), is plotted in the top panel of figure 5 for the WSO measurements, which are made every 10 days. The area shaded gray is between the earliest (lowest ε) reversal which was seen during cycle 23 (green line) and the latest possible reversal date which was the brief return to $p(B_N–B_S) = 0$ during cycle 22 (blue line). (However, notice that the best estimate of the reversal for cycle 22 was at considerably lower ε). The lower panel of figure 5 shows $–pB_{Nf}$ and pB_{Sf} where B_{Nf} and B_{Sf} are the northern and southern polar field variations after they have been passed through a 20nHz low-pass filter to smooth them and remove the annual variation. The vertical lines give the phases of the peaks in 12-point running means of monthly sunspot numbers. Red, blue and green are used to denote cycles SC21, SC22 and SC23 and black is for SC24, using the same ε estimates as in figure 4. Figure 5 shows that the polar fields during SC24 thus far have been weaker than they were in the corresponding phase of the previous 3 cycles. Using $(B_{Nf}–B_{Sf})$ from the WSO data for SC21-SC23 and the corresponding data from Mount Wilson Observatory (MWO) for SC20, along with Babcock's results from HSL for SC19, yields the estimates of the solar cycle phase of the mean polar field reversal, ε_{rev}, given in the Table. It is noticeable that for the odd-numbered cycles ε_{rev} is within 3° (which roughly corresponds to a month) of ε_{max}. However for the even-numbered cycles the polarity reversal took place considerably after the cycle peak. A caveat must be placed on the ε_{rev} value for SC20 because the polar fields were very weak in this cycle, the reversal was extended in nature and the data were noisy which renders defining the reversal very difficult, even in filtered data. Nevertheless it appears that the mean polar field reversal lags the cycle peak by at least 18° (roughly 6 months) for these even-numbered cycles.

The solid black line in the lower panel of figure 5 shows that during SC24, the (filtered) northern polar field has declined steadily and is on the point of reversing at the time of writing (indeed, on 20th April 2012 the Hinode spacecraft team announced that it had reversed), whereas the polar field in the southern hemisphere (dashed black line) has not, as yet, shown any significant decline. Figure 6 explains why this is occurring. The top panel shows the longitudinally-averaged magnetic field as a function of latitude and time: it reveals the butterfly configuration where emerging field loops (and associated sunspots) are in a latitudinal band that migrates equatorward as each cycle progresses. The plot also demonstrates the effects of both Hale's magnetic polarity law (that the polarity of the leading spots is opposite in the two hemispheres and flips from one cycle to the next) and Joy's law (that the trailing spots are at higher latitude than the leading spots). It can be seen that the magnetic field of the trailing spot polarity migrates poleward (on a timescale of about 1 year) and reverses the polarity of the polar regions around the time of sunspot maximum. It is noticeable that the field emerging in the southern hemisphere during the rising phase of SC24 has been much weaker than in the north. This is confirmed by the second panel of figure 6 which shows that the area of sunspot groups in the southern hemisphere have been significantly lower than in the northern (the two became equal for the first time in SC24 during April 2012, on the far right of the plot). Thus the flux emerging and migrating to the pole has been significantly lower in the southern hemisphere and hence SC24 has cancelled the polar field left by SC23 to a notably lesser extent in the south pole compared to the north. The lower panel shows that the cycle onset (as defined by the sharp rise in $<\lambda_{spots}>$) was later in the southern hemisphere and that southern spots have migrated equatorward to a significantly smaller extent. Figure 6 also shows that all these features were also present for SC20, for which ($\varepsilon_{rev} - \varepsilon_{max}$) appears to have been large. Thus SC20 gives us an insight as to how SC24 is likely to evolve, with dominant southern hemisphere spots in the declining phase, a relatively long cycle, and possibly a complex and protracted polar field reversal which is considerably delayed after sunspot maximum. Note, however that SC24 is considerably weaker than was SC20 at the same phase.

Figures 4(b) and 4(c) show that SC24 thus far is evolving in a similar way to the weak cycles SC13 and SC14 (red dots) in 12-month running means of both solar activity (as quantified by *R*) and the near-Earth IMF *B* (after 1965 in-situ spacecraft data are used, before then values are derived from geomagnetic activity as shown in figure 3). The white lines in the middle and right-hand plots of figure 4 are the scaled means of *R* and *B* predicted by the method of *Owens et al.* [2011] from the average behaviour with ε in previous cycles. Note that in the case of *B*, *Owens et al.* only used in-situ spacecraft data for after 1965 and for much of this interval there has been a downward drift in solar cycle means of *B* [*Lockwood and Fröhlich*, 2007]: this causes the predicted solar minimum around ε = 360° to be lower than that around ε = 0°; i.e., a continuing decline is implicit in these predictions. *Owens et al.* estimated a cycle peak sunspot number R_{max} of 65±15 for SC24, consistent with the prior prediction from the weak solar polar fields by *Svalgaard et al.* [2005] but at the lower end of the distribution of other predictions [*Pesnell*, 2008]. The predicted peak in *B* is B_{max} = 5.1±1.0 nT. The grey areas in figure 4 show the 1σ uncertainty ranges around these predictions. Figures 4(e) and 4(f) compare the *Owens et al.* predictions with 12-month running means of observations made thus far and with the predictions for SC24 made from cosmogenic isotopes shown in figure 3. Both *R* and *B* for SC24, thus far, are most consistent with the blue curves ($P[<R]$ and $P[<B]$ ≈ 5-10%), which are consistent with Maunder minimum conditions forming within about 40 years. The same conclusion is obtained from the corresponding plots of cosmic ray fluxes and geomagnetic activity (not shown). It should, however, be noted that figure 4(b) illustrates how the average behaviour of sunspots may not be the best predictor for a weak cycle: the Table shows that ε_{max} has generally been larger for cycles with lower R_{max} (a tendency first noted by *Waldmeier* [1955]) and so the cycle peak could be slightly later and larger than estimated by *Owens et al*. from the average behaviour. However, we note that *Kane* [2008] finds the Waldmeier effect gives only limited additional predictability to the peak sunspot number.

Other indicators of solar activity confirm cycle 24 to be exceptionally weak. As for the near-Earth IMF *B* shown in figure 3, the open solar flux and geomagnetic activity indices (such as aa shown in figure 3) have yet to rise significantly above the levels of even the minima SC21/SC22 and SC22/SC23 and cosmic ray fluxes seen by high-latitude neutron monitors have only fallen slightly below the maxima seen at those times.

Implications for Space Weather and Space Climate

Hence all the indications are that SC24 is revealing a decline in solar activity at the end of a GSM that is unusually rapid compared to past examples the cosmogenic isotope record. If this continued, the Sun would reach Maunder minimum conditions within just 40 years [*Lockwood*, 2010]: as shown by figure 2, this has occurred after just 2 of the 24 GSMs in the last 9300 years. The implications of a continued decline would be that GCR fluxes at Earth will be greater than over recent decades but solar-driven space weather events would be less common: however, there are reasons to think that the Solar Energetic Particle (SEP) events that do occur may more severe than has been the case during the space age thus far [*McCracken et al.*, 2007]. This is because the Alfvén speed in the heliosphere is lower if the magnetic field there is low. Therefore an event ejected into the heliosphere when the open solar flux is low has a higher Alfvén Mach number than an event ejected at the same speed when the open solar flux is high. It is predicted that the energised particle yield is greater when this Mach number is high and so, of two otherwise similar events, higher particle fluence will be seen in the case which follows an interval of lower solar activity. There is some experimental evidence that supports this idea [*Barnard and Lockwood*, 2011; *Barnard et al.*, 2011]. Our engineering solutions to mitigate effects of energetic particles (either galactic or solar in origin) have largely been based on past experience from the space age only. One of the key points about long-term space climate change, just as for the terrestrial effects of global warming, is that past experience will cease to be the best way of arriving at optimum solutions.

As an example of the effects of changing space climate, consider the exposure of passengers and crew to radiation on transpolar flights. Allowed exposure limits vary from nation to nation, but the International Commission on Radiological Protection (ICRP) recommends a 20 mSv limit for the annual exposure of an occupational radiation worker and 1 mSv for the general public. Dosages during a flight depend on path, duration and altitude as well as solar activity. Models such as QARM (which can run be online at http://qarm.space.qinetiq.com/) show that at the solar cycle peaks during the recent GSM, a round trip of two commercial 8-hour transpolar flights would have given a GCR dose of about 0.08 mSv. Thus in excess of 12 such trips in a year would be needed to accumulate the maximum recommended dose for a member of the public. For most of the solar cycle minima during modern times this number fell to about 6 but in the recent low cycle minimum it was 4.5. *Barnard et al.* [2011] show it would fall further to under 3 for Maunder minimum conditions. Although the number of people who undertake 12 such trips in one year is very small, the number making 3 or more will be significantly larger. But of even greater concern are the SEP events. *Mertens et al.* [2010] show that certain flights during the 2003 "Halloween" SEP events would have been exposed to 70% of the recommended annual limit and it is estimated that the largest known event, the "Carrington event" of 1859, would have given up to 20 times the limit [*Cliver and Svalgaard*, 2004]. We have no understanding of why the Carrington event was as large and geoeffective as it appears to have been, but we do know it occurred midway between the last grand minimum (the Maunder minimum) and the recent grand maximum and therefore it is possible we are now moving towards the same set of conditions that gave rise to such a large event.

Implications for Terrestrial Weather and Climate

A question which always arises (not least in the minds of many journalists) is “what would this decline in solar activity mean for climate change?” The one undisputed way in which solar change would influence global climate at Earth’s surface is via a significant change in the total solar irradiance (TSI). However, *Jones et al.* [2012] have used predictions of TSI equivalent to those for *R*, *B* and aa in figure 3 to demonstrate that even a return to Maunder minimum conditions will slow the anthropogenically-driven rise in global mean surface temperatures by only a very small amount. The higher fluxes of GCRs reaching Earth would undoubtedly increase electrical conductivity below the ionosphere which would have some interesting (but difficult to predict) effects on the global thunderstorm electric circuit [*Rycroft and Harrison*, 2011], potentially influencing some climate “teleconnections” between different regions, evidence for which was recently found by *Harrison et al.* [2011]. For over 60 years now, it has also been suggested that there is a mechanism whereby air ions generated by GCRs modulate the formation of cloud and, if these clouds were at low altitude, the predicted rise in GCR fluxes could slow of the global temperature rise or even turn it into a fall. (Note that the reverse effect would be caused by high-altitude cloud). However, it must be stressed that this is a very large “if” indeed as this mechanism remains highly controversial and would most likely have a significant effect only in very clean maritime air where there is a lack of other nucleation centres for the water droplets to grow on. Initial results from the CERN Cloud experiment [*Kirkby et al.*, 2011] have revealed some interesting effects of ionisation on very early droplet growth through sulphuric acid and biological material in the near-surface boundary layer; however, this is certainly not evidence for a similar effect, let alone a sufficient one, in the mid-altitude troposphere that could have climate implications.

Therefore we still have no evidence that there could be a significant solar effect on global scales [see review by *Lockwood*, 2012]; however, that is not to say that there may not be effects in certain regions and certain seasons. In particular, there is growing evidence that regional climates around the north Atlantic in winter may be particularly influenced by the level of solar activity, with lower solar activity giving increased occurrence of jet stream “blocking” events and colder winters in Europe but warmer ones in Greenland [*Woollings et al.*, 2010]. The mechanism appears to involve stratospheric wind changes [*Ineson et al.*, 2011] induced by long-term changes in either solar UV emissions [*Lockwood et al.*, 2010b] or the catalytic destruction of ozone by energetic particles [*Seppälä et al.*, 2009], or both. *Lockwood et al.* [2010a] have used temperature data extending back to the Maunder minimum to infer a statistically significant, influence of the solar activity level on the occurrence of cold winters in the UK.

The Outlook

In conclusion, the Sun does appear to be very quiet in solar cycle 24. The long and low solar cycle minimum that preceded it [*Lockwood*, 2010] is part of a decline in solar activity that began in 1985 [*Lockwood and Fröhlich*, 2007] and a weak cycle 24 would be a continuation of this decline. Weak cycles do tend to peak later than strong ones and the March 2012 storm may yet presage a rise in activity that means the decline is not as rapid as it appears to be at the present time. Nevertheless, it is becoming apparent that some degree of space climate change is underway. As well as offering solar and solar-terrestrial scientists a chance to understand the long-term fluctuations of the solar dynamo, this presents a space-weather engineering challenge as past experience built up during the space age cannot be assumed to apply as the Sun exits the recent grand maximum. As disciplines, solar and solar-terrestrial science have sometimes been accused of “doing more of the same” – a unfair accusation that ignored the great advances made in instrumentation, observation techniques, numerical modelling and physical understanding, but one that now looks particularly short-sighted. The changes in the Sun that are now underway, along with observing opportunities such as Solar Orbiter, Solar Dynamics Observatory, STEREO, and the wide variety of terrestrial observations, mean that scientists now have an exciting chance to understand the longer-term variability of the solar dynamo and its effects. Early detection and understanding of changes in space climate will remain important because they impinge on the design and safe operation of the many man-made systems that are influenced by space weather.

Acknowledgements. The authors are grateful to: Freidhelm Steinhilber of EAWAG, Zürich, for the provision of the heliospheric modulation parameter composite; the staff of the Wilcox Solar and Kitt Peak Observatories for the magnetograph data; the Space Physics Data Facility, NASA/Goddard Space Flight Centre for the Omni2 interplanetary database; the Solar Influences Data Analysis Center (SIDC), of the Royal Observatory of Belgium for the international sunspot numbers; British Geological Survey, Edinburgh, and the UK Space Science Datacentre, RAL, for the most recent geomagnetic data; the ACE magnetometer team for the most recent IMF data and David Hathaway of NASA/Marshall Space Flight centre for the plot of the Kitt Peak data and provision of the Greenwich/USAF sunspot database.

Table. The start/end dates of solar cycles as determined by *Owens et al.* [2011]. The dates, magnitudes (R_{max}) and phases (ε_{max}) of the peaks in 12-month running means of the sunspot number are given. The phases of the polar field reversals (ε_{rev}) are derived from magnetograph data from HSL (SC19), MWO (SC20) and WSO (SC21, SC22 and SC23).

Cycle number	Start Date	End Date	Length (yrs)	Date of maximum	R_{max}	ε_{max} (deg)	ε_{rev} (deg)
SC13	1889.5	1901.2	11.7	1894.1	89	141	
SC14	1901.2	1913.7	12.5	1906.1	65	141	
SC15	1913.7	1923.5	9.8	1917.6	105	143	
SC16	1923.5	1934.0	10.5	1928.2	78	163	
SC17	1934.0	1944.3	10.3	1937.3	121	116	
SC18	1944.3	1954.6	10.3	1947.4	152	109	
SC19	1954.6	1965.0	10.4	1958.2	203	123	121
SC20	1965.0	1976.6	11.6	1968.8	111	119	150±45*
SC21	1976.6	1986.7	10.1	1980.0	165	121	124
SC22	1986.7	1996.8	10.1	1989.6	159	103	121
SC23	1996.8	2009.0	12.2	2000.1	122	103	100
SC24	2009.0	2019.0*	10***	2012.5±0.5**	≥59	125±19**	>120

* uncertain as polar fields are weak, the reversal is extended and noise in data is high
** from mean ± one standard deviation of ε_{max} of cycles 13 to 23
*** estimated from figure 4a

References

Abreu, J. A., et al. (2008), For how long will the current grand maximum of solar activity persist?, *Geophys. Res. Lett.*, **35**, L20109, doi:10.1029/2008GL035442.

Babcock, H. D. (1959) The Sun's Polar Magnetic Field, *Astrophys. J.*, **130**, 364-365.

Barnard, L., and M. Lockwood (2011), A survey of gradual solar energetic particle events, *J. Geophys. Res.*, **116**, A05103, doi:10.1029/2010JA016133.

Barnard, L., et al. (2011), Predicting space climate change, *Geophys. Res. Lett.*, **38**, L16103, doi:10.1029/2011GL048489.

Cliver, E. and L. Svalgaard (2004) The 1859 solar-terrestrial disturbance and the current limits of extreme space weather activity, *Solar Phys.*, **224**, 407–422, doi:10.1007/s11207-005-4980-z.

Dyer, C.S., et al. (2003) Calculations and observations of solar particle enhancements to the radiation environment at aircraft altitudes, *Adv. Space Res.*, **32** (1), 81-93, doi:10.1016/S0273-1177(03)90374-7.

Hapgood, M.A. (2011) Towards a scientific understanding of the risk from extreme space weather, *Adv. Space Res.*, **47** (12), 2059–2072

Hapgood, M.A. and A Thomson (2010) Space weather: Its impact on Earth and implications for business. Lloyd's 360º Risk Insight. London, UK. http://bit.ly/9Pjk9R

Harrison, R.G., et al. (2011) Inferring convective responses to El Niño with atmospheric electricity measurements at Shetland. *Environmental Research Letters*, **6** (4). 044028. doi: 10.1088/1748-9326/6/4/044028

Hathaway, D.H. (2010) The Solar Cycle, *Living Rev. Solar Phys.* **7**, 1. URL (cited on 29 March 2012): http://www.livingreviews.org/lrsp-2010-1

Ineson S. et al. (2011) Solar forcing of winter climate variability in the Northern Hemisphere, *Nature Geosci.*, **4** (11), 753-757. doi: 10.1038/NGEO1282

Jones, G.S. et al., (2012) What influence will future solar activity changes over the 21st century have on projected global near surface temperature changes? *J. Geophys. Res. (Atmos.)*, **117**, D05103, doi:10.1029/2011JD017013.

Kane, R.P. (2008) How useful is the Waldmeier effect for prediction of a sunspot cycle?, J. *Atmos. Sol.-Terr. Phys.*, **70** (11–12), 1533-1540. doi: 10.1016/j.jastp.2008.04.010.

Kirkby, J., et al. (2010) Role of sulphuric acid, ammonia and galactic cosmic rays in atmospheric aerosol nucleation, *Nature*, **476** (7361), 429-U77. doi: 10.1038/nature10343

Lockwood, M. (2010), Solar change and climate: An update in the light of the current exceptional solar minimum, *Proc. R. Soc. A*, **466** (2114), 303–329, doi:10.1098/rspa.2009.0519.

Lockwood, M. (2012) Solar Influence on Global and Regional Climates, Surveys of Geophysics, in press. doi: 10.1007/s10712-012-9181-3

Lockwood, M., and C. Fröhlich (2007) Recent oppositely directed trends in solar climate forcings and the global mean surface air temperature, *Proc. Roy. Soc. A*, **463** , 2447-2460, doi:10.1098/rspa.2007.1880.

Lockwood, M., and M.A. Hapgood (2007) The rough guide to the Moon and Mars, *Astron. & Geophys*., **48**, 11-17.

Lockwood, M., and M.J. Owens (2011) Centennial changes in the heliospheric magnetic field and open solar flux: the consensus view from geomagnetic data and cosmogenic isotopes and its implications, *J. Geophys. Res*., **116**, A04109, doi:10.1029/2010JA016220.

Lockwood, M., R. Stamper, and M. N. Wild (1999), A doubling of the Sun's coronal magnetic field during the past 100 years, *Nature,* **399**, 437–439, doi:10.1038/20867.

Lockwood, M., et al. (2009), The rise and fall of open solar flux during the current grand solar maximum, *Astrophys. J.*, **700** (2), 937–944, doi:10.1088/0004-637X/700/2/937.

Lockwood, M., et al. (2010a) Are cold winters in Europe associated with low solar activity? *Environ. Res. Lett*., **5**, 024001, doi:10.1088/1748-9326/5/2/024001.

Lockwood, M., et al. (2010b) Top-down solar modulation of climate: evidence for centennial-scale change, *Environ. Res. Lett.*, **5**, 034008, doi:10.1088/1748-9326/5/3/034008

Lockwood M., et al. (2011), The persistence of solar activity indicators and the descent of the Sun into Maunder Minimum conditions, *Geophys. Res. Lett.*, **38**, L22105, doi:10.1029/2011GL049811.

McCracken, K. G. (2007) High frequency of occurrence of large solar energetic 219 particle events prior to 1958 and a possible repetition in the near future, *Space Weather,* **5**, S07004, doi:10.1029/2006SW000295.

Mertens, C. J., et al. (2010), Geomagnetic influence on aircraft radiation exposure during a solar energetic particle event in October 2003, *Space Weather*, **8**, S03006, doi:10.1029/2009SW000487.

Owens, M.J., and M. Lockwood (2012) Cyclic loss of open solar flux since 1868: The link to heliospheric current sheet tilt and implications for the Maunder minimum, *J. Geophys. Res.*, **117**, A04102, doi:10.1029/2011JA017193.

Owens, M. J., et al., (2011), How is open solar magnetic flux lost over the solar cycle?, *J. Geophys. Res.*, **116**, A04111, doi:10.1029/2010JA016039.

Owens, M. J., et al. (2011), Solar cycle 24: Implications for energetic particles and long-term space climate change, *Geophys. Res. Lett*., **38**, L19106, doi:10.1029/2011GL049328.

Pesnell, W. D. (2008), Predictions of solar cycle 24, *Sol. Phy*s., **252**, 209–220, doi:10.1007/s11207-008-9252-2.

Rycroft, M. J. and Harrison, R. G. (2012) Electromagnetic atmosphere-plasma coupling: the global atmospheric electric circuit. *Space Science Reviews*, in press, ISSN 0038-6308

Seppälä , A., et al. (2009) Geomagnetic activity and polar surface air temperature variability, *J. Geophys. Res.*, **114**, A10312, doi:10.1029/2008JA014029

Solanki, S.K., et al. (2000) Evolution of the Sun's large-scale magnetic field since the Maunder minimum, *Nature*, **408**, 445–447.

Steinhilber, F., et al. (2008), Solar modulation during the Holocene, *Astrophys. Space Sci. Trans.*, **4**, 1–6, doi:10.5194/astra-4-1- 008.

Svalgaard, L., et al. (2005), Sunspot cycle 24: Smallest cycle in 100 years?, *Geophys. Res. Lett.*, **32**, L01104, doi:10.1029/2004GL021664.

Usoskin, I. G., et al. (2002), A physical reconstruction of cosmic ray intensity since 1610, *J. Geophys. Res*., **107**(A11), 1374, doi:10.1029/2002JA009343.

Waldmeier, M., (1955) Ergebnisse und Probleme der Sonnenforschung. 2nd Ed., Leipzig, p. 154.

Weiss, N.O. and M. J. Thompson (2009) The Solar Dynamo, *Space Sci. Rev.*, **144** (1-4), 53-66, doi: 10.1007/s11214-008-9435-z

Woollings, T.G. et al. (2010) Enhanced signature of solar variability in Eurasian winter climate, *Geophys. Res. Lett.*, **37**, L20805, doi:10.1029/2010GL044601.

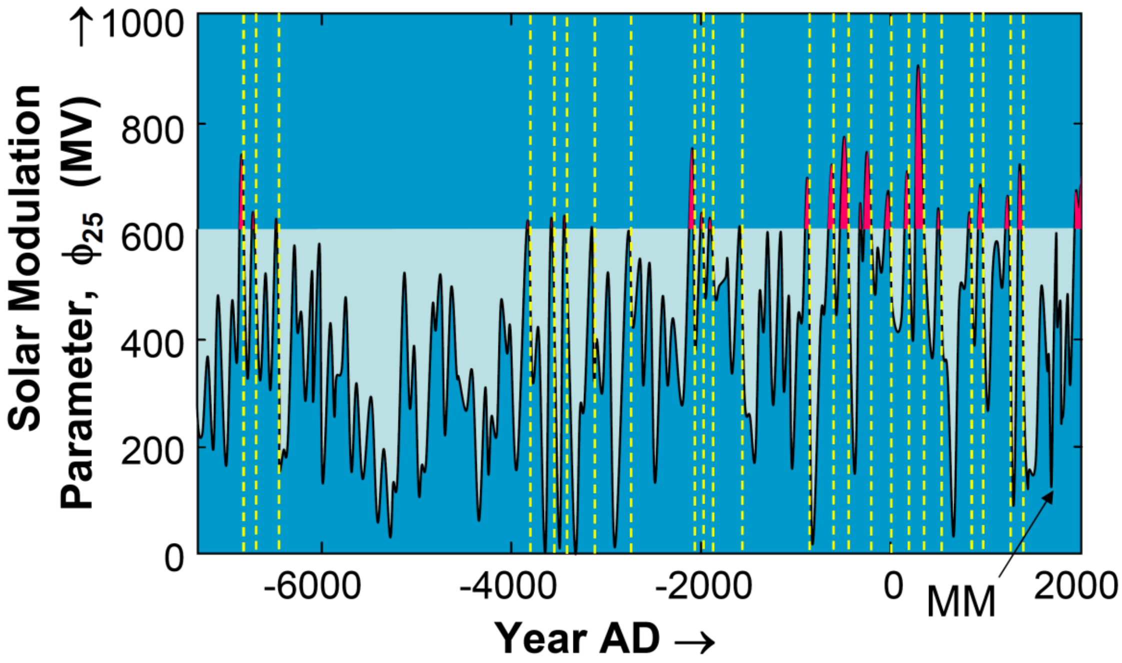

Figure 1. The composite of 25-year means of the heliospheric modulation parameter, ϕ_{25}, derived from ^{10}Be abundances in ice cores and modern neutron monitor data by *Steinhilber et al.* [2008]: ϕ quantifies the shielding of the Earth from Galactic Cosmic Rays (GCRs) by the Sun. The areas shaded red are Grand Solar Maxima (GSMs), defined to be when ϕ_{25} exceeds the 610 MV. The yellow dashed lines mark the ends of the 24 such GSMs detected in the 9300-year record. The Maunder Minimum is labelled MM.

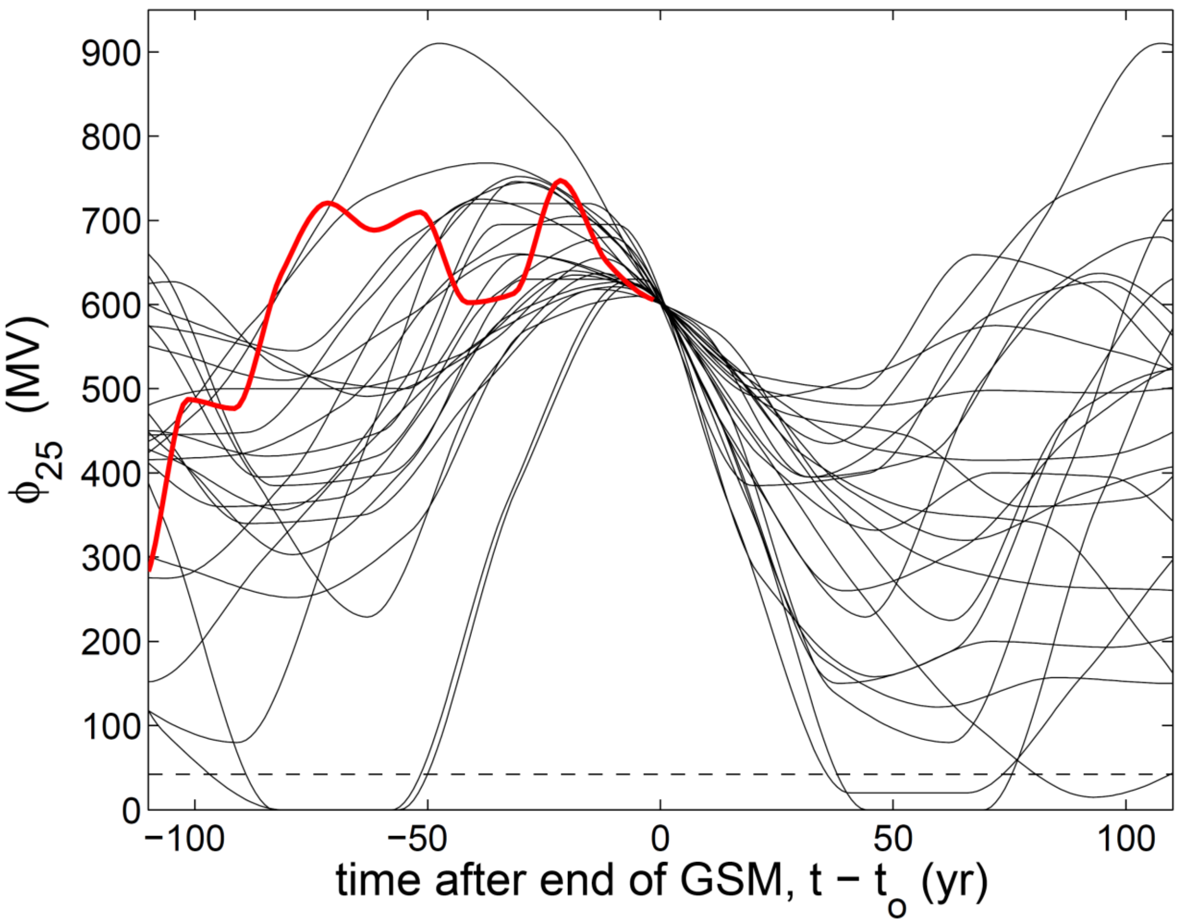

Figure 2. Composite of the variations in ϕ_{25} around the ends of the GSMs defined by the dashed yellow lines in figure 1 (at times t_o). The red curve is the variation for the recent GSM, extrapolated to the present day using neutron monitor data, and shows the recent decline which began in 1985. The horizontal dashed line is the level during the Maunder minimum.

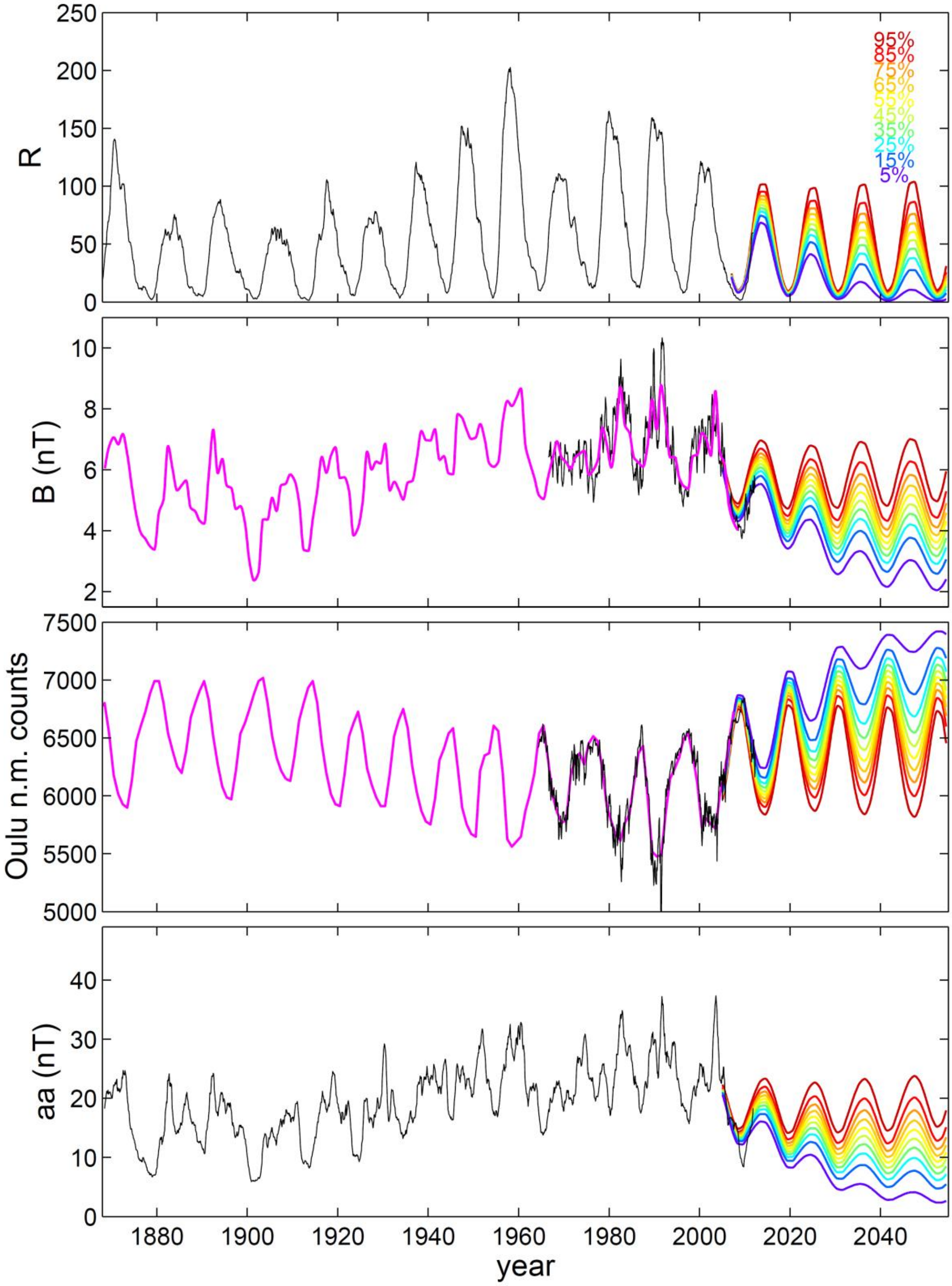

Figure 3. Observed past and predicted future variations of (from top to bottom): sunspot number, *R*; interplanetary magnetic field strength at Earth, *B*; cosmic ray counts by the Oulu neutron monitor; and the aa geomagnetic index. The black lines are monthly averages of

observations (a 12-month running mean smooth has been applied to R and aa). The mauve line in the second panel is the reconstruction of annual means of *B* from geomagnetic data by *Lockwood et al.*, [2009] and that in the third panel from the reconstruction of ϕ by *Usoskin et al.* [2002]. The red-to-blue lines show predicted variations of annual means at various probabilities, made from the 9300-year cosmogenic isotope composite by *Steinhilber et al.* [2008] using the procedure developed by *Lockwood* [2010] and *Barnard et al.* [2011]. In the top panel the red to blue lines show the values of *R* which have a probability of being exceeded of $P[\geq R] = 1 - P[<R] = [0.05:0.1:0.95]$. Corresponding predictions are given in the other two panels.

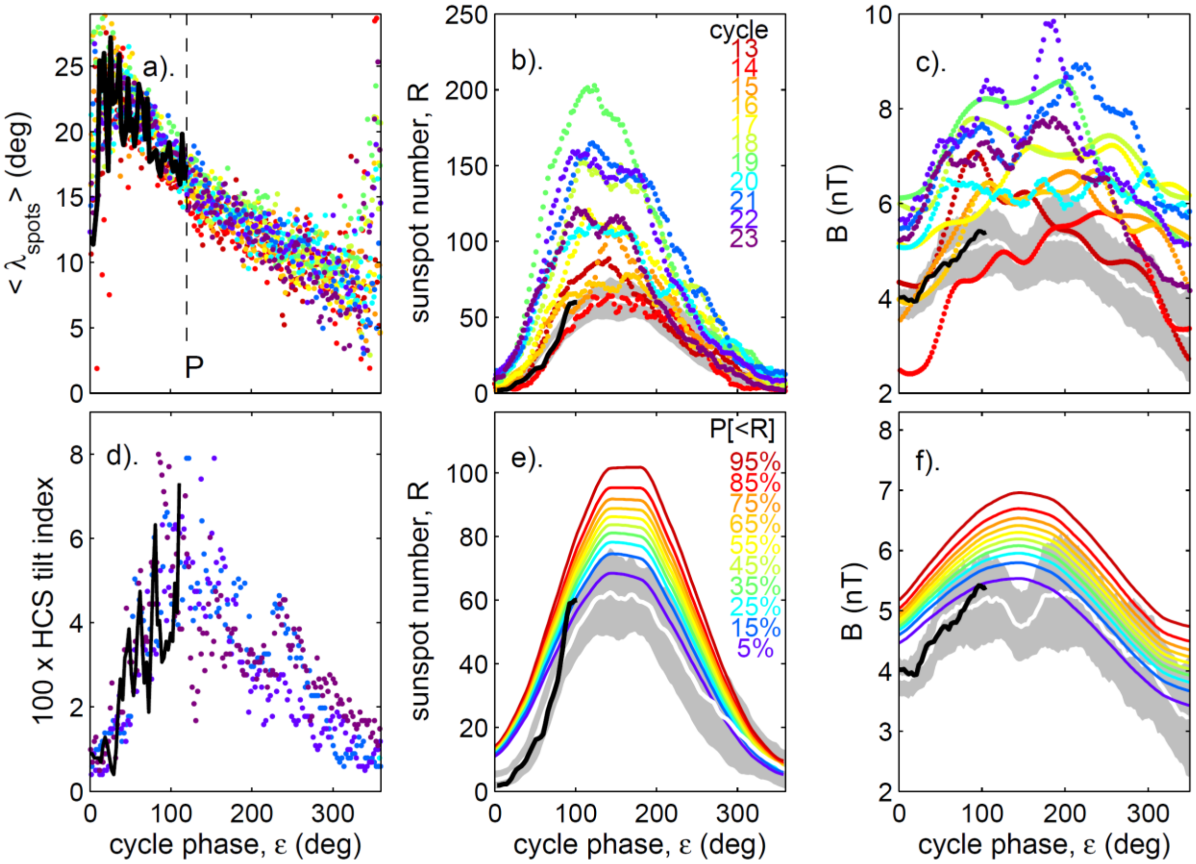

Figure 4. Evolution of solar cycles. (a). The variation of the monthly mean heliographic latitude of sunspots $<\lambda_{spots}>$ with the phase of the solar cycle, ε, for SC13 to SC23 (red to mauve dots). The black line shows SC24 data to date, for the best-fit length of this cycle of 10 years which yields ε = 120° for 1st May 2012 (vertical dashed line labelled P). (d) is the corresponding plot of Carrington Rotation means of the heliospheric current sheet tilt index (note these data are only available after 1976 and so cover SC21-SC24 only). The other panels compare 12-month running means of predicted and observed variations for SC24: (b) and (e) show sunspot number, *R*; and (c) and (f) show the near-Earth interplanetary magnetic field, *B*. The white lines are the means predicted by the method of *Owens et al.* [2011] and the surrounding grey area is the ±1σ uncertainty band. The dots in (b) and (c) are the values for previous cycles and the red-to-blue

coloured lines in (e) and (f) are the analogue forecasts from cosmogenic isotope data, as presented in the top two panels of figure 3.

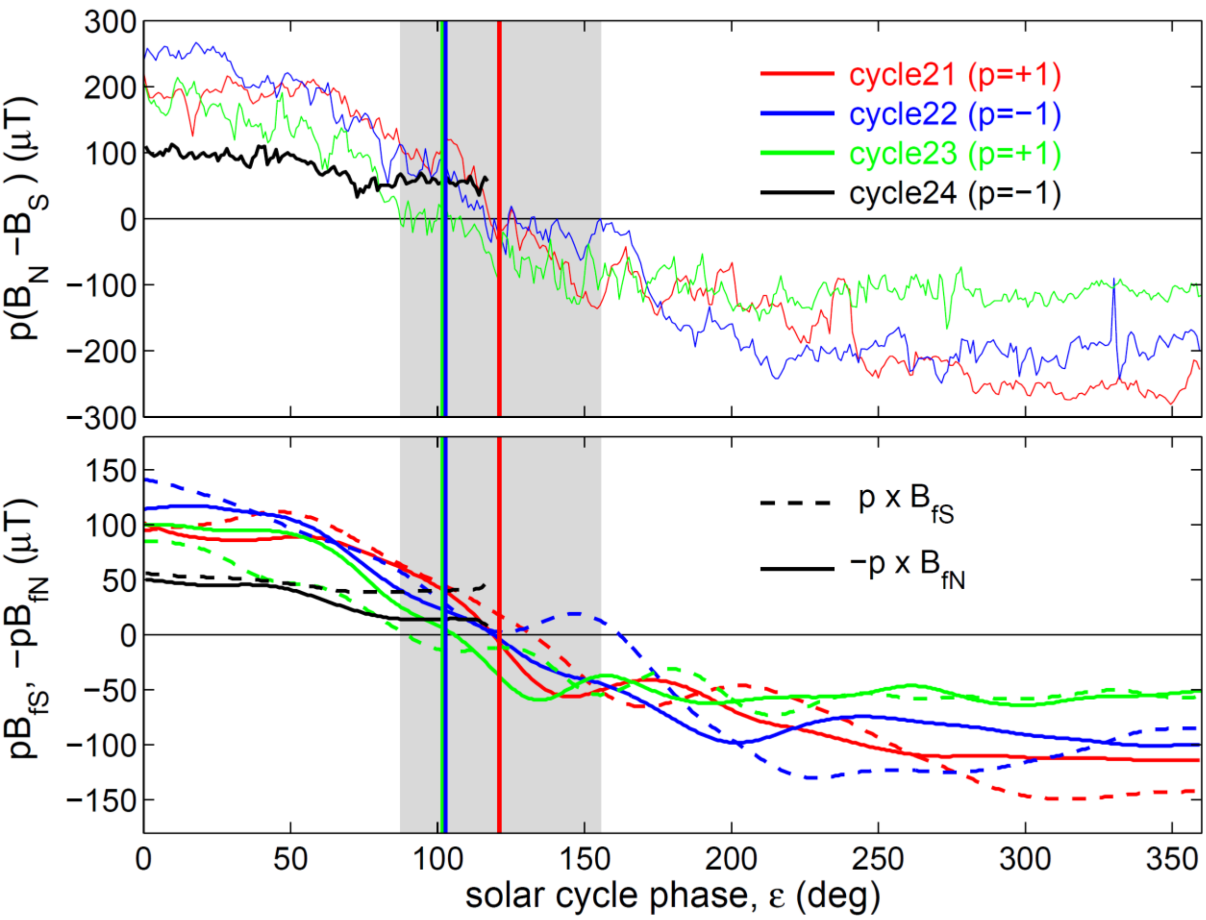

Figure 5. Solar polar fields observed by the magnetograph at Wilcox Solar Observatory (WSO) during solar cycles 21-24. The top panel shows the difference between the two polar fields, $p(B_N - B_S)$ as a function solar cycle phase (ε, determined as in figure 4), where B_N and B_S are the average fields seen over the north and south solar poles, respectively, and $p = +1$ for odd-numbered cycles $p = -1$ for even ones. The reversals all occur within the grey band and the phases of the peak sunspot number in 12-month running means are given by the vertical lines. The lower panel shows $-pB_{Nf}$ (solid lines) and pB_{Sf} (dashed lines) as a function of ε where B_{Nf} and B_{Sf} are the B_N and B_S data that have been passed through a 20nHz low-pass filter. In both panels, red, blue, green and black denotes solar cycles SC21, SC22, SC23 and SC24, respectively.

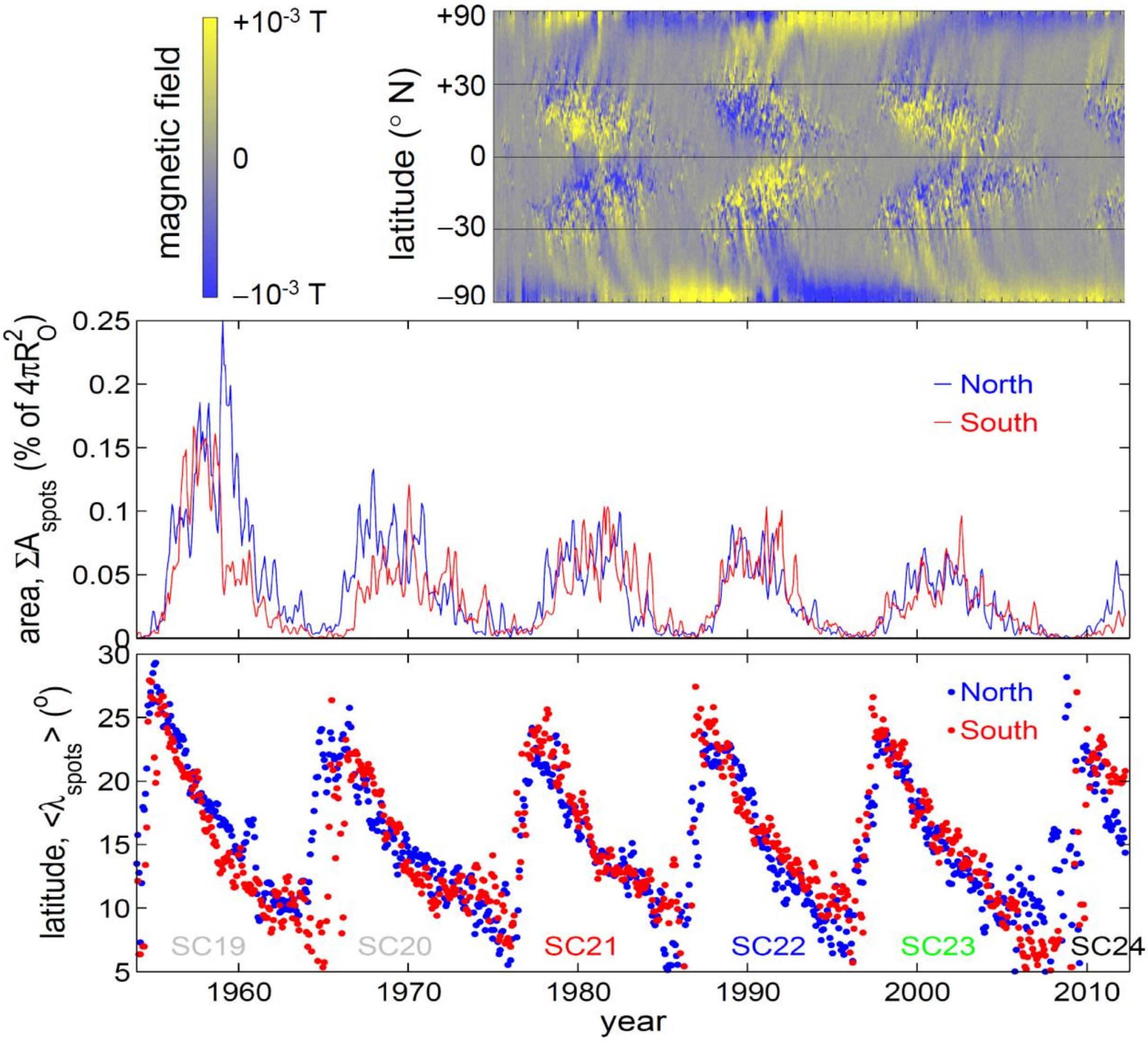

Figure 6. Comparison of sunspot activity in the north and south solar hemispheres. The top panel is the "magnetic butterfly diagram" and shows the longitudinally-averaged magnetic field measured by the Kitt Peak Observatory (KPO) magnetograph as a function of latitude and time (plot courtesy of D. Hathaway, NASA/Marshall Space Flight Center). The middle panel shows the total area of sunspot groups and the lower panel the mean latitude of the spots. In both of the lower panels, blue is for the northern hemisphere and red is for the southern.